


Volume 50, issue 5, May 2008 ISSN 0010-938X



# CORROSION SCIENCE

The Journal on Environmental Degradation of Materials and its Control  
Editor-in-Chief: G. T. BURSTEIN, University of Cambridge, U.K.  
An Official Journal of the Institute of Corrosion

### CONTENTS

H. MIYAMOTO, K. HARADA, T. MINGAKI, A. VINOGRADOV and S. HANIMOTO	1215	Corrosion of ultra-fine grained copper fabricated by equal-channel angular pressing
D.-I. KIM, H.-C. KWON and H. P. KIM	1221	Effects of the solution temperature and the pH on the electrochemical properties of the surface oxide films formed on Alloy 600
J. P. LABRÉ, J. LEDION and F. HUI	1228	Infrared spectrometry for solid phase analysis: Corrosion rusts
B. JEGDIĆ, D. M. DRAŽIĆ and J. P. POPIĆ	1235	Open circuit potentials of metallic chromium and austenitic 304 stainless steel in aqueous sulphuric acid solution and the influence of chloride ions on them
N. SEDIQUAN, N. OCHIAI, N. PERIERE and B. THIBOLLET	1245	Variation of carbon steel corrosion rate with flow conditions in the presence of an inhibitive formulation
S. L. ZELINSKA, D. R. RAMMER and D. S. STONE	1251	Electrochemical corrosion testing of fasteners in extracts of treated wood
L. M. PALOMBO, P. H. SUEGAMA, I. V. AOKI, M. F. MONTESOR and H. G. DE MELO	1258	Electrochemical study of modified non-functional bis-silane layers on Al alloy 2024-T3
A. B. M. MUBBER RAHMAN, S. KUMAR and A. R. GIBSON	1267	The speciation of Si and other alloying elements in the oxide surface film of galvanically corroded weld fusion zone of laser welded AA6061 aluminium alloy
B.-I. SKEFVYARS, R. BACKMAN, M. HUPA, K. SALMENROSA and E. VAKKILAINEN	1274	Corrosion of superheater steel materials under alkali salt deposits. Part 1: The effect of salt deposit composition and temperature
N. C. ROSERO-NAVARRO, S. A. PELLICE, A. DURAN and M. APARICIO	1283	Effects of Ce-containing sol-gel coatings reinforced with SiO <sub>2</sub> nanoparticles on the protection of AA2024
J. CHEN, J. WANG, E. HAN, J. DONG and W. KE	1292	States and transport of hydrogen in the corrosion process of an AZ91 magnesium alloy in aqueous solution
T. NISHIMURA	1306	Rust formation and corrosion performance of Si- and Al-bearing ultrafine grained weathering steel

*Contents continued on outside back cover*  
<http://www.elsevier.com/locate/corsci>

This article appeared in a journal published by Elsevier. The attached copy is furnished to the author for internal non-commercial research and education use, including for instruction at the authors institution and sharing with colleagues.

Other uses, including reproduction and distribution, or selling or licensing copies, or posting to personal, institutional or third party websites are prohibited.

In most cases authors are permitted to post their version of the article (e.g. in Word or Tex form) to their personal website or institutional repository. Authors requiring further information regarding Elsevier's archiving and manuscript policies are encouraged to visit:

<http://www.elsevier.com/copyright>



## Effects of Ce-containing sol–gel coatings reinforced with SiO<sub>2</sub> nanoparticles on the protection of AA2024

N.C. Rosero-Navarro, S.A. Pellice, A. Durán, M. Aparicio \*

*Instituto de Cerámica y Vidrio (CSIC), Campus de Cantoblanco, 28049 Madrid, Spain*

Received 11 July 2007; accepted 31 January 2008

Available online 23 February 2008

### Abstract

A hybrid organic–inorganic self-healing coating for anticorrosive protection of AA2024 was developed through the sol–gel method. Combination of permeability, provided by a methacrylate-silica hybrid matrix, with hardness and density of silica nanoparticles, allowed obtaining a coating material where the diffusion of Ce ions occurred at the same time that an anticorrosive physical barrier was developed. Electrochemical impedance spectra (EIS) on coated samples showed an increase of the impedance modulus at 0.01 Hz as a function of immersion time in a 3.5 wt% NaCl solution. Self-healing effect was verified by impedance fitting through the evolution of resistive and capacitive parameters of the equivalent circuits.

© 2008 Elsevier Ltd. All rights reserved.

**Keywords:** A. Rare earth elements; A. Aluminium; B. EIS; C. Sol–gel; C. Hybrid coatings

### 1. Introduction

Aluminium alloys are widely used as structural materials because of their low densities and excellent mechanical properties. However, these alloys are subjected to corrosion when exposed to the environment, which is a highly important topic for aerospace and automotive industries. Chromate conversion coatings (CCCs) provide an excellent protection mechanism against the localized corrosion. CCCs present self-healing behaviour after superficial damage; a scratch or defect appearing in the film can be protected by migration of soluble Cr (VI) species from the coating that precipitate on the surface healing the defect [1]. However CCCs are extremely dangerous for human health and generate serious problems of environmental contamination. In fact, the European Parliament and the Council on end-of-life vehicles foresaw the total elimination of Cr based coatings before 1st July 2007 [2]. There-

fore, it is necessary to find a replacement that supplies an enough protection against corrosion.

AA2024 (Al, 4.4% Cu, 1.5% Mg, 0.6% Mn) is the most common aluminium alloy used in aerospace applications and it is rather susceptible to localized corrosion as a result of its heterogeneous microstructure. The inhomogeneous distribution of Cu associated with intermetallic particles gives high strength and toughness to the structure but, on the other hand, makes it very vulnerable to rising temperatures that decrease the mechanical properties. Thus, any treatment to improve the corrosion resistance of AA2024 should not rise above 120 °C to avoid dissolution of the intermetallic particles [3]. This fact makes useless the inorganic sol–gel coatings which provide excellent barrier properties as anticorrosive films because they need thermal treatments of densification at temperatures higher than 350 °C [4,5]. Furthermore, the requirements of the aircraft industry impose very rigorous conditions for coatings. Due to the possibility of corrosion by the presence of scratches, micropores and areas with low cross-linking density, a simple barrier against corrosion is not enough to protect the aircraft's structural alloys. In fact, the actual requirement

\* Corresponding author. Tel.: +34 91 7355840; fax: +34 91 7355843.  
E-mail address: [maparicio@icv.csic.es](mailto:maparicio@icv.csic.es) (M. Aparicio).

is a protective coating that, besides providing a good barrier against corrosion, can be resistant to small defects through a self-healing process provided by inhibitors incorporated in the coatings.

A possible alternative for replacing CCCs is the development of hybrid organic–inorganic sol–gel coatings, which can be densified at low temperatures without affecting the microstructure and mechanical properties of the AA2024 substrate. The control of the synthesis parameters, incorporation of different organic monomers and inorganic nanoparticles allows obtaining materials with the desired properties like density and hydrophilic character [6,7]. Many authors have focused their works on hybrid organic–inorganic sol–gel coatings as protection for AA2024-T3 at low temperatures [8–13]. Barriers against corrosion can be prepared using alkylalkoxides and epoxy-functionalized alkoxides with thermal treatments between room temperature and 80 °C [8–10]. Other authors [11–13] have incorporated different compounds, such as inorganic salts or organic inhibitors with the purpose of obtaining a self-healing effect. The inhibitors incorporated in the film should migrate and precipitate producing a passivating deposit where the defect was originated. Rare earths, like Ce and La, are well-known corrosion inhibitors. Ce ions form insoluble hydroxides which can work as cathodic inhibitors [14], they have a low toxicity and are relatively abundant in nature [15–19].

The objective of this work was the development of new self-healing hybrid coatings designed to produce an effective barrier as well as an appropriate support for passivating agents. In the present study, hybrid organic–inorganic sols were developed from tetraethoxysilane (TEOS) and 3-methacryloxypropyl trimethoxysilane (MPS) using SiO<sub>2</sub> nanoparticles to improve mechanical and barrier properties and a source of Ce(III), cerium nitrate, as inhibitor. MPS permits an increase in the maximum thickness of hybrid coatings through a stress relaxation induced in the silica structure [6]. The self-healing effect was analysed by impedance measurements (EIS) as a function of immersion time in a NaCl standard solution.

## 2. Experimental

The precursor sols were synthesized employing 3-methacryloxypropyl trimethoxysilane (MPS, ABCR, 98%), tetraethoxysilane (TEOS, ABCR, 98%), colloidal SiO<sub>2</sub> (Levasil 200A, Bayer, aqueous suspension 40 wt%, particle size 20 nm, pH 9) and cerium nitrate (Ce(NO<sub>3</sub>)<sub>3</sub> · 6H<sub>2</sub>O, Aldrich, 99%) as a source of Ce (III).

Three different sols were prepared from TEOS and MPS incorporating SiO<sub>2</sub> nanoparticles. TM–SiO<sub>2</sub> sol was prepared keeping the molar ratio TEOS/MPS of 65/35 adding the colloidal silica suspension at a 35 mol% with respect to alkoxides. Hydrolytic condensation was catalysed at room temperature with HNO<sub>3</sub> concentrated at a 0.6 vol% reaching a pH between 2 and 3. A final silica concentration of 250 g l<sup>-1</sup> was obtained by diluting with ethanol. TM–SiO<sub>2</sub> sol was doped with Ce (III) salt at the end of the synthesis

keeping Ce/Si molar ratios of 5/95 and 10/90, for the TM–SiO<sub>2</sub>–5Ce and TM–SiO<sub>2</sub>–10Ce sols, respectively.

Glass slides (2.5 × 7 cm<sup>2</sup>) and AA2024-T3 aluminium alloy (5 × 7 cm<sup>2</sup>) were used as substrates. Aluminium alloy was exposed to a three-step cleaning procedure using Metaclean T2001 (Chemie Vertrieb Hannover GmbH & Co KG), Turco Liquid Aluminetch Nr. 2 (Turco Chemie GmbH) and Turco Liquid Smutgo NC (Turco Chemie GmbH).

Coatings were obtained by dip-coating at different withdrawal rates between 20 and 40 cm/min on glass slides and AA2024 aluminium alloy. The films were dried at room temperature and densified during 120 min at 120 °C in air with a heating rate of 10 °C/min. The coating thickness was measured by profilometry (Talystep, UK).

AC impedance spectra for bare and coated metal substrates were performed in 3.5 wt% NaCl solution with a conventional three-electrode cell. A saturated calomel reference electrode (SCE) and a platinum wire as counter-electrode were used in the tests. The surface area of the test coupons (as the working electrode) exposed to the electrolyte was 3.14 cm<sup>2</sup>. Impedance measurements (EIS) were performed using a Gamry FAS2 Femtostat at different times of immer-

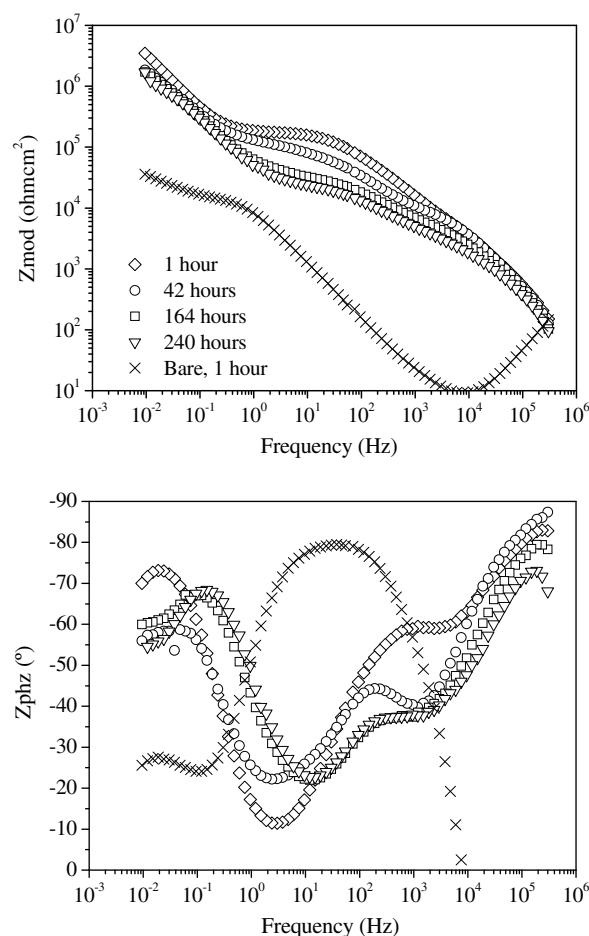


Fig. 1. Impedance diagrams (Bode plots) for the bare AA2024 after one hour of immersion and the alloy with TM–SiO<sub>2</sub> coatings after different immersion times in 3.5 wt% NaCl solution.

sion in the electrolyte. The tests started by recording the electrode potential with time. When the corrosion potential remained stable, a sinusoidal ac signal of 5 mV (rms) amplitude at the open circuit potential (OCP) was applied to the electrode over the frequency ranged from  $3 \times 10^5$  Hz down to  $10^{-2}$  Hz. Each value was obtained as the mean value of five measurements in a logarithmic sweep of frequencies (10 points per logarithmic unit). Impedance fitting was performed using Gamry Echem Analyst software.

AA2024-T3 coated samples, before and after electrochemical tests, were evaluated by optic and scanning electron microscopy (HITACHI S-4700 field emission). Elemental chemical analysis of the coatings was performed by Energy Dispersive X-ray Spectroscopy (EDX, NORAN system six) connected to the FE-SEM.

### 3. Results and discussion

The sols were transparent and colourless, with viscosity values around 5 cP. Coatings after thermal treatment are transparent. The Ce-free coating was colourless and the Ce-doped ones were slightly yellow. The thickness was 3.7, 4.3 and 4.0  $\mu\text{m}$  for coatings prepared without Ce, and doped with 5% and 10% of cerium, respectively.

Fig. 1 shows the impedance diagrams (Bode plots) for the bare AA2024 after one hour of immersion and the alloy with TM-SiO<sub>2</sub> coatings after different immersion times in 3.5 wt% NaCl solution. The EIS results are interpreted through a two-layer coating model with an inner thin layer composed of natural aluminium oxide, and the outer sol-gel coating. The phase angle curve of the bare alloy

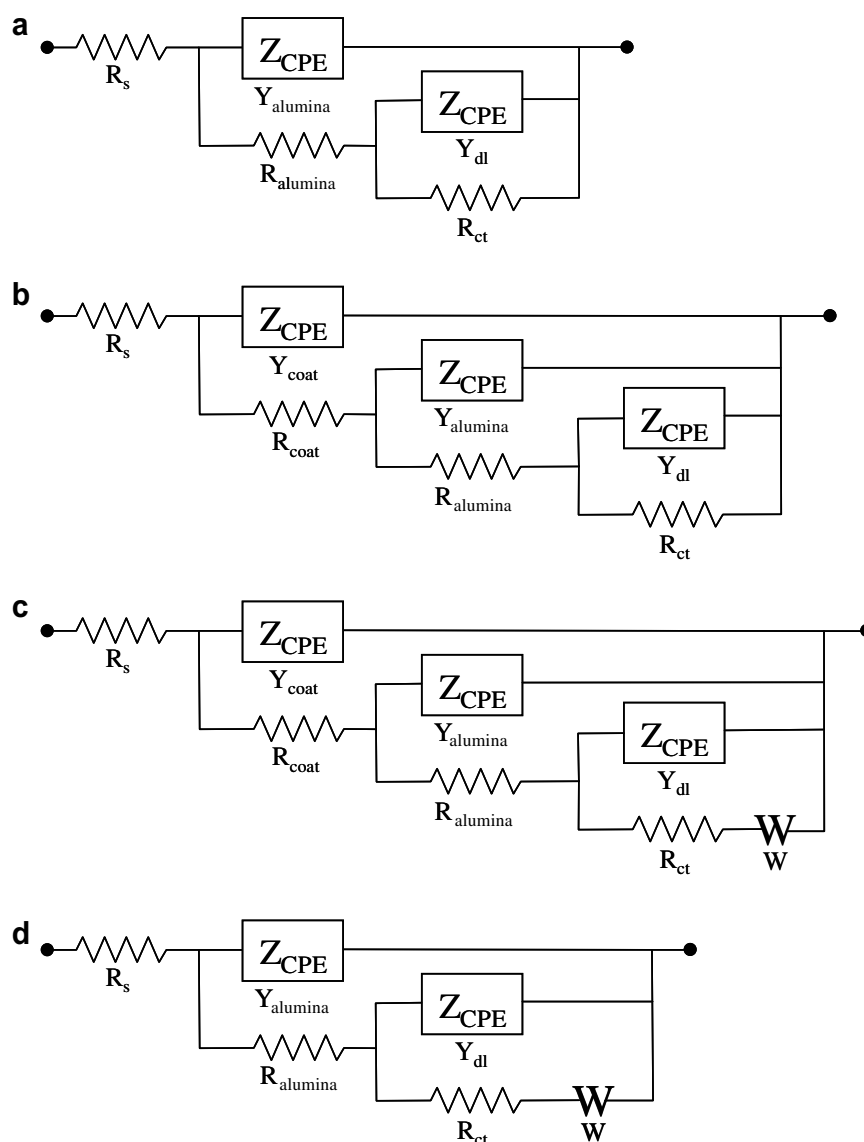


Fig. 2. Equivalent circuits used to fit the EIS spectra: (a) Bare AA2024 after 1 h of immersion; (b) AA2024 with TM-SiO<sub>2</sub> coatings after 1 and 42 h of immersion; (c) AA2024 with TM-SiO<sub>2</sub> coatings after 164 and 240 h of immersion, and AA2024 with TM-SiO<sub>2</sub>-5Ce coatings after 1, 41, and 114 h of immersion; (d) AA2024 with TM-SiO<sub>2</sub>-5Ce coatings after 215 h of immersion, and AA2024 with TM-SiO<sub>2</sub>-10Ce coatings after all immersion times.

presents two time constants at 30 and 0.015 Hz, assigned to the intermediate aluminium oxide layer and the electron charge transfer process from corrosion, respectively [20]. The incorporation of the sol–gel coating originates the presence of a new time constant at higher frequencies (above  $10^5$  Hz) associated with the sol–gel layer. This coating also leads to an increase of the impedance modulus at 0.01 Hz of two orders of magnitude as a consequence of the additional barrier functionality provided. However, Bode plots of coated samples after only one hour of immersion showed signals of corrosion activity by the presence of a time constant at 0.02 Hz. A porous structure of the sol–gel coating should explain this behaviour. The other two time constants at  $10^3$  and  $2.10^5$  Hz correspond to the intermediate layer and the sol–gel coating, respectively. A relatively open structure like this can be adequate for the objective of combination of barrier properties and self-healing effect when an inhibitor such as cerium is incorporated in the coating.

The increase of the immersion time produced a slow deterioration of the corrosion protection system. The total impedance at 0.01 Hz decreases slightly with time as a first signal of degradation. As well, the plateau observed in the impedance plot between 1 and 100 Hz, associated with the contribution of the resistances assigned to the NaCl solution, sol–gel coating and intermediate layer, decrease with immersion time, also indicating coating degradation. The reduction of phase angle of the two higher frequency time constants with immersion time indicates a less capacitive response due to the permeation of the solution through the pores of the sol–gel coating and intermediate layer. At lower frequencies, the phase angle also decreases with immersion time, suggesting the occurrence of diffusion processes within pores in the coating. Nyquist plots (not shown) for 164 and 240 h show the characteristic diffusion tails with an angle of  $45^\circ$  attached to the semicircle at low frequency. In spite of the continuous and slow deterioration, the system maintains a good level of protection after 240 h of immersion [21].

The interpretation of impedance spectra was performed using numerical fitting. In the simulation, the constant phase element (CPE) was used instead of an “ideal” capacitor to explain the deviations from ideal behaviour. The impedance of a CPE ( $Z_{CPE}$ ) can be defined by [22]

$$Z_{CPE} = (1/Y)/(j\omega)^a \quad (1)$$

The parameters correspond to the frequency ( $\omega$ ), pseudo-capacitance ( $Y$ ), and the parameter  $a$  associated to the system homogeneity. When this equation describes a capacitor,  $a = 1$  and  $Y = C$  (the capacitance). For a CPE, the exponent  $a$  is less than one.

The equivalent circuits used to model all impedance curves are displayed in Fig. 2.  $R_s$ , the resistance of the electrolyte, has very low values being usually ignored.  $R_{coat}$  is the resistance of the sol–gel coating, considered to be due to the formation of ionically conducting paths in the coating.  $Y_{coat}$  is the pseudo-capacitance of the sol–gel coating,

and  $R_{alumina}$  and  $Y_{alumina}$ , the resistance and pseudo-capacitance associated with the thin natural aluminium oxide layer.  $R_{ct}$  is the resistance describing the corrosion of the metal substrate in contact with the ionically conducting paths.  $Y_{dl}$  is the double-layer pseudo-capacitance formed in the metal-electrolyte interface.  $W$  is a Warburg or pseudo-impedance element included to model increasing ionic conductivity due to the corrosion process. When the coating is thick enough, as in this case, the Warburg impedance is described by [22]

$$Z_w = (1/Y)/(j\omega)^{1/2} \quad (2)$$

These equivalent circuits are used in several papers [20,23,24] to fit impedance spectra in the case of aluminium alloys covered with hybrid silica sol–gel coatings.

The variation of resistances and capacitances with the immersion time obtained from the analysis of impedance spectra for TM–SiO<sub>2</sub> coated AA2024 samples using the equivalent circuits of Fig. 2 are shown in Fig. 3. Errors from numerical fitting appear in the plot. The values of “Goodness of Fit” obtained with Gamry Echem Analyst software indicate an average error below 10%. The resis-

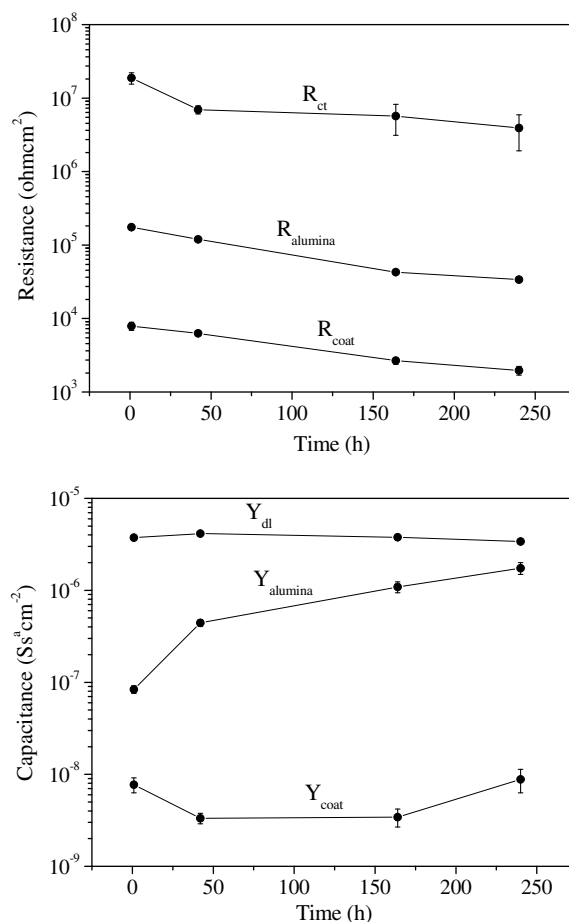


Fig. 3. Resistances and capacitances values of AA2024 alloy protected with TM–SiO<sub>2</sub> coatings as a function of immersion time in 3.5 wt% NaCl solution. Errors obtained from numerical fitting for each data are incorporated in the plot.

tance of the coatings usually decreases with time of exposure due to the permeation of electrolyte through the pores of the coating. This trend has been previously observed in the literature and the slope is a consequence of the quality of the coating formed on the alloy surface [25,26]. Resistances of sol-gel coating and intermediate layer show a slow reduction with time up to the end of the test as a consequence of the existence of open porosity. In spite of this porous structure,  $R_{ct}$  maintains high values along all the immersion time confirming the good barrier properties of the coating. The value of  $R_{ct}$  for the bare alloys was  $2 \times 10^5$  Ohms  $\text{cm}^2$ , much lower than that of coated alloy as a consequence of the difference in the exposed area of metal to the solution. The capacitance of the coatings ( $C_{\text{coating}}$ ) can be written as

$$C_{\text{coating}} = \epsilon \epsilon_0 A / t \quad (3)$$

$A$  is the area exposed,  $\epsilon$  is the dielectric constant of the coating,  $\epsilon_0$  is the permittivity of vacuum ( $8.85 \times 10^{-12}$  F/cm), and  $t$  is the thickness. As  $\epsilon$  of coatings is generally small, usually an order of magnitude smaller than that of water ( $\epsilon = 80$ ), the penetration of water into the coating should increase its capacitance [22,27]. Fig. 4 shows photographs of the tested areas of coated samples after the EIS tests. TM-SiO<sub>2</sub> coatings (Fig. 4a) presents a transparent and

almost intact coating with only scarce isolate pitting. This coating provides a good barrier, although the initiation of the pitting can not be stopped due to the absence of a corrosion inhibitor.

The incorporation of cerium ions in the coating TM-SiO<sub>2</sub>-5Ce originates a significant change in the corrosion behaviour of AA2024 alloy. Fig. 5 shows the Bode plots of the alloy AA2024 with TM-SiO<sub>2</sub>-5Ce coatings after different immersion times in 3.5 wt% NaCl solution. The values of impedance at 0.01 Hz are almost two orders of magnitude lower than those obtained with sol-gel coatings without cerium. This change is an indication of a coating with a higher content of defects. The presence of cerium ions in the hybrid structure of the coating generates additional porosity with an increase of conducting paths [23]. Although it is not so evident as in the case of coatings without cerium, the phase angle curves at 1, 41 and 114 h of immersion maintain the three time constants already observed with TM-SiO<sub>2</sub> coatings and assigned to sol-gel coating, intermediate aluminium oxide layer and electron charge transfer process. The curve at 215 h of immersion does not show the time constant above  $10^5$  Hz because of the presence of an artefact of the measurement. Like in TM-SiO<sub>2</sub> coatings, the presence of diffusion processes through pores is exhibited in a phase angle shift of  $45^\circ$  in

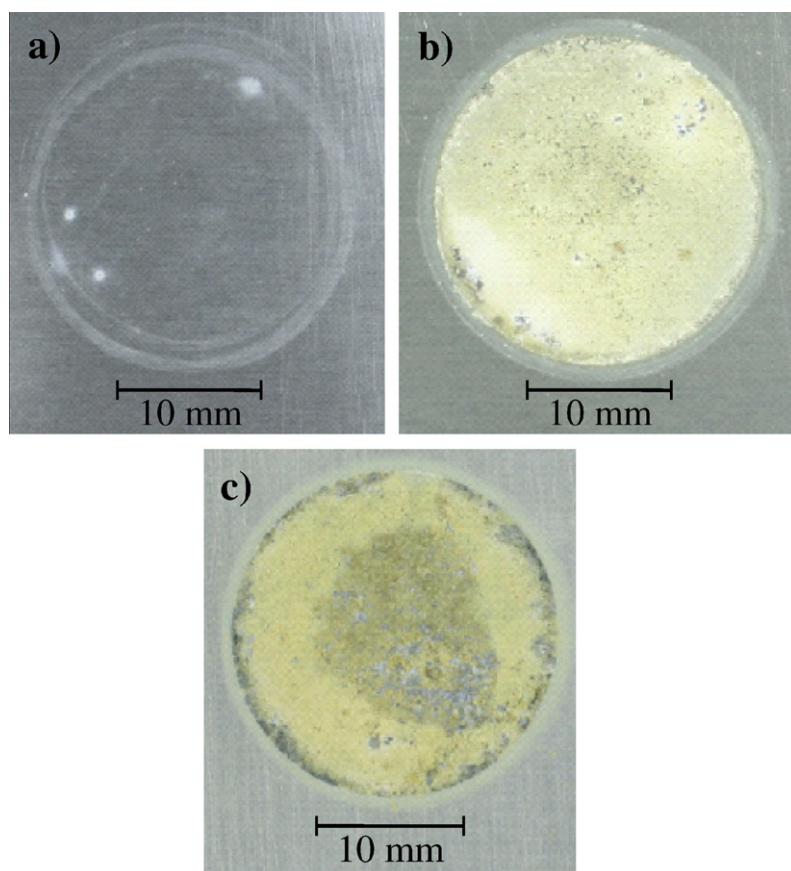


Fig. 4. Photographs of the tested areas of samples with coatings after the EIS – immersion time analysis: (a) TM-SiO<sub>2</sub> coating, (b) TM-SiO<sub>2</sub>-5Ce coating, and (c) TM-SiO<sub>2</sub>-10Ce coating.

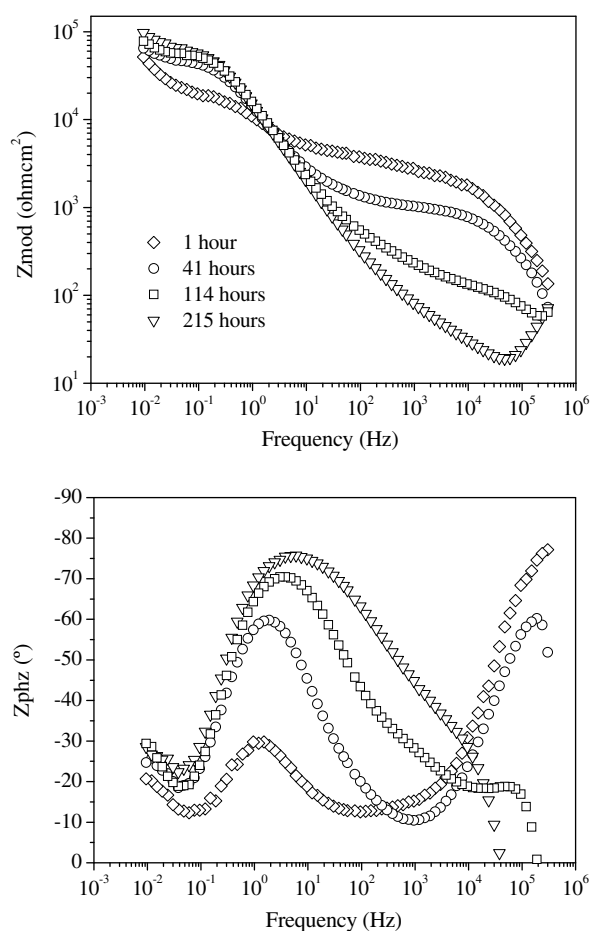


Fig. 5. Impedance diagrams (Bode plots) for the bare AA2024 alloy protected with TM-SiO<sub>2</sub>-5Ce coatings after different immersion times in 3.5 wt% NaCl solution.

the phase plot and a decreasing slope in the impedance modulus plot at lower frequencies. The reduction of the impedance at around 10<sup>3</sup> Hz is also a signal of the deterioration of the barrier functionality provided by the sol-gel coating and intermediate layer. Although the incorporation of cerium ions has induced a partial degradation of the coating as barrier, an inhibition action has been provided. A first signal of this new anticorrosion mechanism is the increase of the impedance modulus at 0.01 Hz with immersion time, contrary to that observed in coatings without cerium. As resistances assigned to the sol-gel coating and intermediate layer decrease with immersion time, the rise of the impedance at 0.01 Hz can only be associated with a significant increasing of the resistance describing the corrosion of the metal substrate ( $R_{ct}$ ). In theory, the value of  $R_{ct}$  would be the most appropriate parameter for monitoring the protective properties of the coating as the corrosion rate of the underlying metal can be estimated from the Stern–Geary equation [27]. On the other hand, the variation of the time constant related to the corrosion process show an unusual behaviour. The increase of the phase angle from 30° for 1 h to almost 80° after 215 h of immersion indicates a more capacitive behaviour. Both factors

(increase of  $R_{ct}$  and phase angle) indicate the presence of deposits or precipitates well adhered and with enough density to reduce the area affected by corrosion.

The role of cerium ions on the corrosion protection has been associated with the precipitation of cerium hydroxides/oxides on cathode sites [28]. Some papers [29–32] describe the partial oxidation of Ce<sup>3+</sup> to Ce<sup>4+</sup> ions, and the further precipitation of CeO<sub>2</sub> through the formation of intermediate species as Ce(OH)<sub>2</sub><sup>2+</sup> or Ce(OH)<sub>3</sub>.

The numerical fitting of the impedance curves of TM-SiO<sub>2</sub>-5Ce coatings to equivalent circuits (Fig. 2) provides the variation of resistances and capacitances displayed in Fig. 6. Errors for each parameter are included in the figure. The change of both parameters confirms the hypothesis described above. While resistances associated with alumina layer and sol-gel coating show a quicker decreasing with immersion time compared with coatings without cerium, resistance of charge transfer process presents an increase from 1.8 × 10<sup>4</sup> to 6.2 × 10<sup>4</sup> Ohms cm<sup>2</sup> after 1 and 215 h of immersion, respectively.

In spite of this effect, this value is much lower than that of coatings without cerium indicating that a single layer

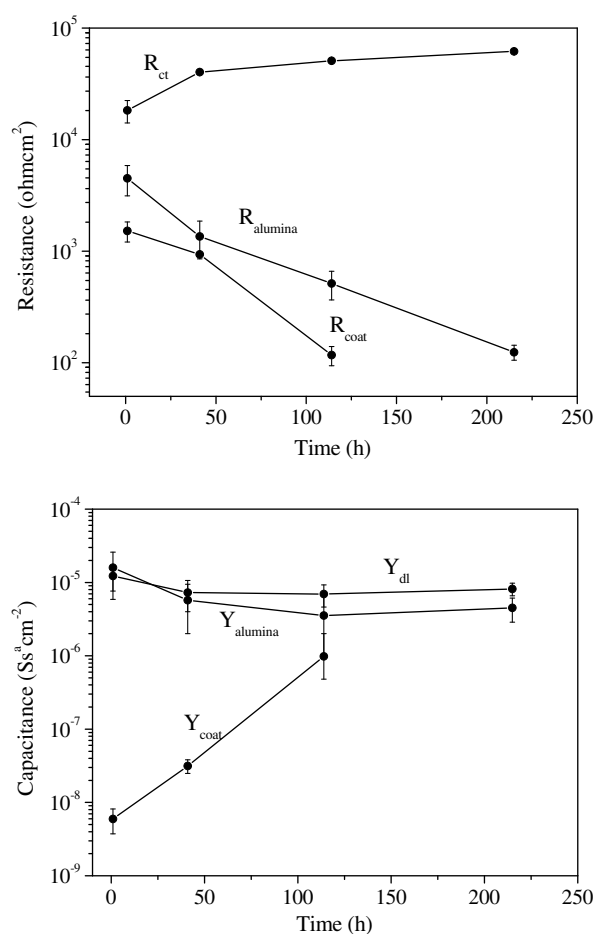


Fig. 6. Resistances and capacitances values of AA2024 alloy protected with TM-SiO<sub>2</sub>-5Ce coatings as a function of immersion time in 3.5 wt% NaCl solution. Errors obtained from numerical fitting for each data are incorporated in the plot.

doped with cerium is not enough to provide suitable corrosion protection to the metal substrate. The capacitance of the sol-gel coating illustrates a very quick increase with time, indicating a fast water uptake and thus, the rapid deterioration of the coating doped with cerium. This behaviour has been associated with blister formation and local loss of adhesion [25,26]. Fig. 4b shows a photograph of the sample protected with the TM-SiO<sub>2</sub>-5Ce coating after the EIS-time test. Well adhered yellowish precipitates all over the test area can be observed. The analysis of this sample by FE-SEM shows a partial detachment of the sol-gel coating and the presence of a granulated and inhomogeneous coating on the aluminium substrate (Fig. 7). The particles have an average size of 50 nm and seem to be formed from smaller particles. The EDS analysis of areas with higher concentration of particles shows a general increasing of the cerium content compared with the nominal composition. The Ce concentration changes along the sample, probably due to preferential concentration of cerium in some sites and inhomogeneous thickness. Macroscopic pits such as those observed on samples protected with coatings without cerium were not detected. This behaviour can be attributed to the self-healing effect provided by cerium.

Here, a doubt about the association of the impedance increasing at 0.01 Hz with immersion time could exist, although the photographs and the SEM study have demonstrated a precipitation of products with a high content of cerium. A new publication (included as Ref. [26]) has just appeared in the literature dealing with this subject. In this article, the authors demonstrate using a SVET technique that the increase of impedance at low frequency with immersion time can be associated with the self-healing effect provided by an inhibitor incorporated to the sol-gel coating. In order to reject that the impedance increasing with immersion time could be related only with the formation of corrosion products, the evolution of impedance

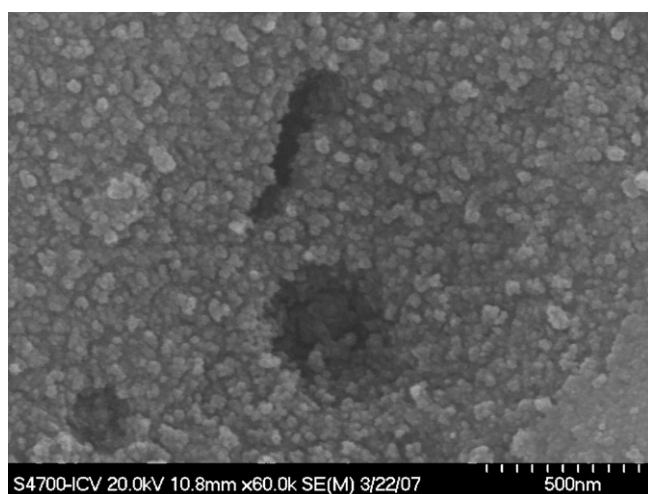


Fig. 7. FE-SEM micrograph of a sample protected by a TM-SiO<sub>2</sub>-5Ce coating after the EIS-time test (215 h of immersion in NaCl 3.5 wt%).

spectra of bare substrates with immersion time is presented in Fig. 8. The phase angle plot shows two time constants assigned to the alumina layer and corrosion process. The increase of immersion time originates a reduction of the impedance modulus as a consequence of the corrosion degradation.

Bode plots of alloy AA2024 protected with TM-SiO<sub>2</sub>-10Ce coatings after different immersion times in 3.5 wt% NaCl solution are displayed in Fig. 9. The figure shows the same tendency observed with 5% cerium containing coatings. The increase of cerium content to 10% produces a greater and faster degradation of the barrier properties. This behaviour can be observed in the reduction of impedance values at 0.01 Hz, and it is a consequence of the higher porosity of this coating. The phase angle plot reflects curves with only two time constants at around 2 and 200 Hz associated with the corrosion process and alumina layer, respectively. No evidence of a time constant related to the sol-gel coating can be observed likely due of its high porosity. Signals of diffusion process at low frequencies can be deduced by the phase angles shift to 45°. The increase of impedance at 0.01 Hz with immersion time from the very beginning can be attributed to the self-healing effect provided by cerium atoms. The fitting to equivalent circuits

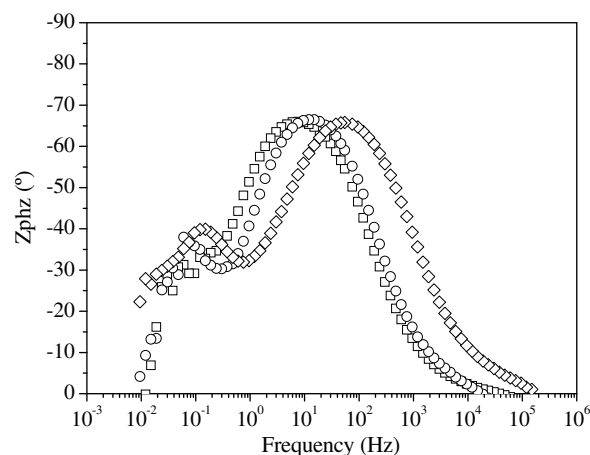
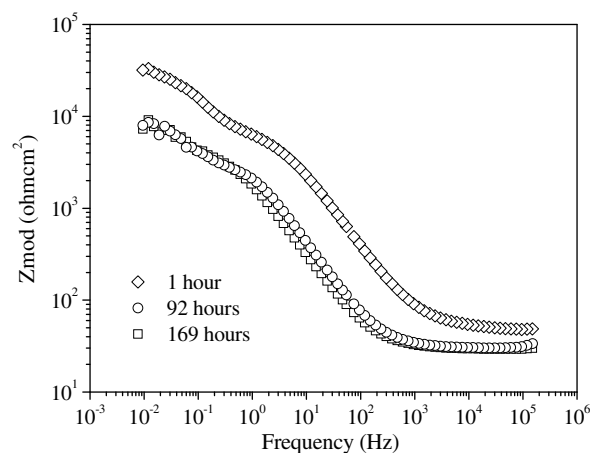


Fig. 8. Impedance diagrams (Bode plots) for the bare AA2024 after different immersion times in 3.5 wt% NaCl solution.



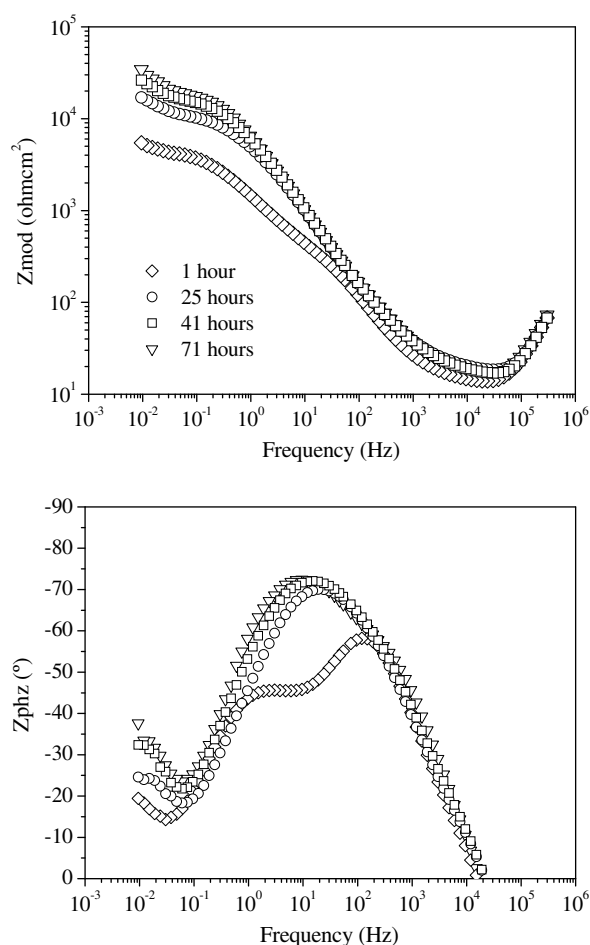


Fig. 9. Impedance diagrams (Bode plots) for the AA2024 alloy protected with TM-SiO<sub>2</sub>-10Ce coatings after different immersion times in 3.5 wt% NaCl solution.

(Fig. 2) indicates a rise of  $R_{ct}$  and a reduction of  $R_{alumina}$  (not shown) in a similar way than that observed with TM-SiO<sub>2</sub>-5Ce coatings.  $R_{ct}$  of TM-SiO<sub>2</sub>-10Ce coatings increases from  $3.6 \times 10^3$  to  $1.5 \times 10^4$  Ohms cm<sup>2</sup> for 1 and 71 h of immersion. Fig. 4c presents a photograph of the sample protected with the TM-SiO<sub>2</sub>-10Ce coating after the EIS-time test. Although yellowish precipitates can be observed as clear signals of self-healing effect, a higher pitting concentration is observed in comparison with samples with TM-SiO<sub>2</sub>-5Ce coating (Fig. 4b). The porosity of coatings with 10% cerium is excessive, this implicating a low barrier effect and a rapid permeation of the electrolyte to the substrate. Thus the corrosion kinetics is very fast and the inhibitor content is not enough to heal all the pitting produced. Although these results confirm the self-healing effect behaviour provided by those coatings, cerium contents higher than 5 mol% generates an excessive porosity that limits drastically the barrier properties of these coatings.

Both barrier functionality and self-healing effect have been achieved in a single hybrid coating. The incorporation of cerium ions to the coating induces an inhibition action, but its inclusion reduces significantly the barrier properties.

Further work is oriented to the combination of two coatings: an inner one doped with cerium ions and an outer coating without cerium with only barrier functionality. Separating both functions it should be possible to emphasize both mechanisms, by producing a barrier coatings with higher density and inhibitor doped coating with a higher content of cerium to produce self-healing effect.

#### 4. Conclusions

The incorporation of cerium (III) to hybrid sol-gel coatings of TEOS – MPS – colloidal SiO<sub>2</sub> generates self-healing effect promoting the corrosion protection of AA2024T3 alloy. On the other hand, the cerium provokes a porous structure that diminish the barrier proprieties of the layers respecting to those without cerium. After confirming the inhibitor effect of Ce ions, a double-layer system combining self-healing and barrier functionalities is under development.

#### Acknowledgements

Authors acknowledge the funding provided by the European Community (MULTIPROTECT project: “Advanced environmentally friendly multifunctional corrosion protection by nanotechnology”, Contract N° NMP3-CT-2005-011783) and by the Spanish Ministry of Education and Science (project MAT2006-4375). The authors thank Laura Peláez her assistance with the experimental technique.

#### References

- [1] J. Zhao, G. Frankel, R.L. McCreery, Corrosion protection of untreated AA-2024-T3 in chloride solution by a chromate conversion coating monitored with Raman spectroscopy, *J. Electrochem. Soc.* 145 (1998) 2258–2264.
- [2] Official Journal of the European Union. Directive 2000/53/EC.
- [3] R.B. Ross, *Metallic Materials Specification Handbook*, Chapman & Hall, London, 1992.
- [4] Y. Castro, A. Durán, R. Moreno, B. Ferrari, Thick sol-gel coatings produced by electrophoretic deposition, *Adv. Mater.* 7 (2002) 505–508.
- [5] A. Durán, Y. Castro, M. Aparicio, A. Conde, J.J. de Damborenea, Protection and surface modification of metals with sol-gel coatings, *Int. Mater. Rev.* 52 (2007) 175–192.
- [6] S. Pellice, P. Galliano, Y. Castro, A. Durán, Hybrid sol-gel coatings produced from TEOS and  $\gamma$ -MPS, *J. Sol-Gel Sci. Technol.* 28 (2003) 81–86.
- [7] S.A. Pellice, R.J.J. Williams, I. Sobrados, J. Sanz, Y. Castro, M. Aparicio, A. Durán, Solutions of hybrid silica microgels as precursors of sol-gel coatings, *J. Mater. Chem.* 16 (2006) 3318–3325.
- [8] T.L. Metroke, J.S. Gandhi, A. Apblett, Corrosion resistance properties of Ormosil coatings on 2024-T3 aluminum alloy, *Prog. Org. Coat.* 50 (2004) 231–246.
- [9] T.L. Metroke, O. Kachurina, E.T. Knobbe, Spectroscopic and corrosion resistance characterization of amine and super acid-cured hybrid organic-inorganic thin films on 2024-T3 aluminum alloy, *Prog. Org. Coat.* 44 (2002) 185–199.
- [10] Y. Liu, D. Sun, H. You, J.S. Chung, Corrosion resistance properties of organic-inorganic hybrid coatings on 2024 aluminum alloy, *Appl. Surf. Sci.* 246 (2005) 82–89.
- [11] A.N. Khranova, N.N. Voevodin, V.N. Balbysheva, R.A. Mantz, Sol-gel-derived corrosion-protective coatings with controllable

- release of incorporated organic corrosion inhibitors, *Thin Solid Films* 483 (2005) 191–196.
- [12] M.L. Zheludkevich, R. Serra, M.F. Montemor, K.A. Yasakau, I.M. Miranda Salvado, M.G.S. Ferreira, Nanostructured sol–gel coatings doped with cerium nitrate as pre-treatments for AA2024-T3 Corrosion protection performance, *Electrochim. Acta* 51 (2005) 208–217.
- [13] N.N. Voevodin, N.T. Grebasch, W.S. Soto, F.E. Arnold, M.S. Donley, Potentiodynamic evaluation of sol–gel coatings with inorganic inhibitors, *Surf. Coat. Technol.* 140 (2001) 24–28.
- [14] M. Bethencourt, F.J. Botana, J. J. Calvino, M. Marcos, M.A. Rodriguez-Chacon, Lanthanide compounds as environmentally-friendly corrosion inhibitors of aluminium alloys: a review, *Corros. Sci.* 40 (1998) 1803–1819.
- [15] M.A. Arenas, M. Bethencourt, F.J. Botana, J. de Damborenea, M. Marcos, Inhibition of 5083 aluminium alloy and galvanised steel by lanthanide salts, *Corros. Sci.* 43 (2001) 157–170.
- [16] M.A. Arenas, A. Conde, J.J. de Damborenea, Cerium: a suitable green corrosion inhibitor for tinplate, *Corros. Sci.* 44 (2002) 511–520.
- [17] A.E. Hughes, R.J. Taylor, B.R.W. Hinton, L. Wilson, XPS and SEM characterization of hydrated cerium oxide conversion coatings, *Surf. Interf. Anal.* 23 (1995) 540–550.
- [18] B.R.W. Hinton, Corrosion inhibition with rare earth metal salts, *J. Alloy Compd.* 180 (1992) 15–25.
- [19] M.W. Kendig, R.G. Buchheit, Corrosion inhibition of aluminum and aluminum alloys by soluble chromates chromate coatings and chromate-free coatings, *Corrosion* 59 (2003) 379–400.
- [20] M.L. Zheludkevich, R. Serra, M.F. Montemor, I.M. Miranda Salvado, M.G.S. Ferreira, Corrosion protective properties of nanostructured sol–gel hybrid coatings to AA2024-T3, *Surf. Coat. Technol.* 200 (2006) 3084–3094.
- [21] G.W. Walter, A review of impedance plot methods used for corrosion performance analysis of painted metals, *Corros. Sci.* 26 (1986) 681–703.
- [22] Gamry Instruments, FAS2 Femtostat, Physical Electrochemistry and Equivalent Circuit Elements, Inc. USA, 2003.
- [23] M.L. Zheludkevich, D.G. Shchukin, K.A. Yasakau, H. Möhwald, M.G.S. Ferreira, Anticorrosion coatings with self-healing effect based on nanocontainers impregnated with corrosion inhibitor, *Chem. Mater.* 19 (2007) 402–411.
- [24] S.V. Lamaka, M.L. Zheludkevich, K.A. Yasakau, R. Serra, S.K. Poznyak, M.G.S. Ferreira, Nanoporous titania interlayer as reservoir of corrosion inhibitors for coatings with self-healing ability, *Prog. Org. Coat.* 58 (2007) 127–135.
- [25] F. Andreatta, P. Aldighieri, L. Paussa, R. Di Maggio, S. Rossi, L. Fedrizzi, Electrochemical behaviour of ZrO<sub>2</sub> sol–gel pre-treatments on AA6060 aluminium alloy, *Electrochim. Acta* 52 (2007) 7545–7555.
- [26] M.L. Zheludkevich, K.A. Yasakau, A.C. Bastos, O.V. Karavai, M.G.S. Ferreira, On the application of electrochemical impedance spectroscopy to study the self-healing properties of protective coatings, *Electrochem. Commun.* 9 (2007) 2622–2628.
- [27] A. Amirudin, D. Thierry, Application of electrochemical impedance spectroscopy to study the degradation of polymer-coated metals, *Prog. Org. Coat.* 26 (1995) 1–28.
- [28] W. Trabelsi, P. Cecilio, M.G.S. Ferreira, M.F. Montemor, Electrochemical assessment of the self-healing properties of Ce-doped silane solutions for the pre-treatment of galvanised steel substrates, *Prog. Org. Coat.* 54 (2005) 276–284.
- [29] A. Pepe, M. Aparicio, S. Ceré, A. Durán, Preparation and characterization of cerium doped silica sol–gel coatings on glass and aluminum substrates, *J. Non-Cryst. Solids* 348 (2004) 162–171.
- [30] A. Pepe, M. Aparicio, A. Durán, S. Ceré, Cerium hybrid silica coatings on stainless steel AISI 304 substrate, *J. Sol–Gel Sci. Technol.* 39 (2006) 131–138.
- [31] A.J. Aldykiewicz Jr., A.J. Davenport, H.S. Isaacs, Studies of the formation of cerium-rich protective films using X-ray absorption near-edge spectroscopy and rotating disk electrode methods, *J. Electrochem. Soc.* 143 (1996) 147–154.
- [32] M.A. Arenas, J.J. Damborenea, Growth mechanisms of cerium layers on galvanised steel, *Electrochim. Acta* 48 (2003) 3693–3698.